JOURNAL OF GEOPHYSICAL RESEARCH, VOL. 99, NO. C3, PAGES 5249–5262, MARCH 15, 1994

Surface gravity waves at equilibrium with a steady wind

Roman E. Glazman

Jet Propulsion Laboratory, California Institute of Technology, Pasadena

Abstract. Observations of wave fields' spatial evolution and of gravity wave spectra $S(\omega)$ are analyzed on the basis of the data reported by several research groups as well as on a 2-year data set of wind and wave measurements by stationary National Oceanic and Atmospheric Administration buoys near the Hawaiian Islands. We seek to clarify the role of the wave energy advection (with the wave group velocity) in the overall energy balance. This advective transfer appears to be no less important than the local (breaking wave induced) dissipation as a factor of wind-wave equilibrium. The advection is found to manifest itself in the shape of wave spectra by reducing the rate at which the spectral density of the wave energy, $S(\omega) \sim \omega^{-p}$, falls off as the frequency increases away from the spectral peak. This and other conclusions are derived by comparing the field observations with theoretical predictions of the weak turbulence theory for a spatially inhomogeneous, statistically stationary, wave field. The observations also indicate that the typical wave age $\xi = C_0/U$ in the open ocean is much greater than the limiting value 1.2 attributed to the "fully developed sea." Although the observed spectra can be approximated by a power law with a single "effective" exponent, this apparent exponent, p, is found to depend on the wave age. At high ξ and at frequencies below the generation range, $-p$ tends to -3 rather than the value of $-11/3$ predicted by the Zakharov-Zaslavskii theory. This deviation is interpreted as pointing to a nonconservative nature of the inverse cascade, the latter including a leakage of energy to low-wavenumber modes. Dependence of the overall effective exponent on ξ is shown to be responsible for variation in the coefficients b, B, c, C appearing in empirical fetch laws, such as $\xi = C\tilde{x}^c$ and $e = B\tilde{x}^b$, where $\tilde{x}$ and e are the dimensionless fetch and wave energy, respectively.

1. Introduction

One of the outstanding issues in dynamics of the upper ocean is the physical mechanism through which energy and momentum are transferred from wind to various components of ocean circulation. Air-sea interaction involves generation of surface gravity waves, which may play an important role in air-sea exchanges on larger scales. The present, primarily experimental, study is focused on weakly nonlinear wave-wave interactions and wave dispersion as possible factors of energy and momentum exchanges between the wave field and larger-scale oceanic motions. In particular, we shall stress that at a sufficiently high degree of sea development, characteristic to open ocean waves, the regime of air-sea interaction is markedly different from that observed for a poorly developed sea state in which the wave energy is dissipated locally.

In general, dissipation of the wave energy can occur through a variety of mechanisms effective in different spectral bands. However, the main dissipation mechanism currently assumed in most wave studies and in wave models is the breaking of short gravity waves. The source functions parameterizing this mechanism are essentially empirical. The same is true with respect to the wind input source function. One particular requirement used in wave models' design is the convergence to the fully developed sea (FDS) as the wind fetch and duration grow. The FDS state parameterized by the Pierson-Moskowitz (P-M) spectrum [*Pierson and Moskowitz*, 1964] is characterized by a limiting wave age ξ (defined in equation (1)) of about 1.2, which means that the phase velocity of the spectral peak waves cannot noticeably exceed the characteristic wind velocity (at a height of, say, 10 m). The FDS state (a statistically stationary and spatially homogeneous wave field) is believed to be a result of local balance between wind input and high-frequency dissipation of wave energy.

The view presented above was recently challenged [*Glazman*, 1991b], and in the present work we provide experimental data and theoretical arguments indicating significant problems with the FDS concept in its present form. In particular, we suggest that under open ocean conditions, the breaking wave dissipation may actually play only a secondary role in the overall energy balance. More effective mechanisms extracting energy and momentum from waves should be sought at low frequencies at which the waves interact with larger-scale motions (such as internal waves, Langmuir circulations, mesoscale eddies, etc.) through the radiation stress and, possibly, mean sea level gradient. In other words, the balance between the wind input and wave dissipation is essentially nonlocal. Furthermore, we demonstrate that characteristic wave age values as high as 3 are not only feasible but are rather common to wind-driven waves in an open ocean, and the P-M spectrum, while appropriate under certain specific conditions, does not represent any fundamental limit on the wave evolution process. Our discussion of these conceptual issues, presented in sections 5–7, is based on the following experimental approach.

Paper number 93JC03317.
0148-0227/94/93JC-03317$05.00

Limiting our consideration to a special case of a statistically stationary wave field at equilibrium with a steady wind, we carefully selected situations characterized by relatively simple wave generation conditions that can be described in the framework of the time-independent equations for energy and action transfer in a spatially evolving wave field (this framework is presented in the next section). This allowed us to avoid as much as possible various adjustable parameters and empirical source functions. The experimental data employed came from different sources: the spatial evolution of the wave field is analyzed on the basis of field observations reported by several independent groups (summarized in Table 1), and the shape of wave spectra is studied based on the Hawaiian buoy data procured from the National Oceanic and Atmospheric Administration (NOAA) (section 3).

Analyzing jointly the shape of the wave spectrum (section 4) and the spatial evolution of the wave field (section 5), we were able to express various coefficients appearing in fetch laws (9)–(11) as functions of "external" parameters of the wave spectrum (sections 5 and 6) and thus interpret the experimental data on the basis of the equations for energy and action transfer. Moreover, we found that many empirical results, including the dependence of the spectrum shape on the wave age, can be explained rather consistently based on the integrated transfer equations with a single "adjustable" parameter, the (constant) coefficient for the wind input, C_q. Experimental data on this coefficient are reviewed in Appendix B.

Owing to the intrinsic slowness of tetrad wave-wave interactions, the characteristic spatial scale for the wave field evolution is of the order of 100 km. Therefore experimental studies of the processes addressed in the present work cannot be conducted in wave tanks, lakes, or other confined basins. Moreover, being interested in deep-water gravity waves, one must make sure that the characteristic depth is at least of the order of the dominant wave length. The latter, as our data show, attains a few hundred meters.

In the next section, the necessary background information on equilibrium wave spectra is reviewed.

2. Basic Relations for Developed Sea Spectra: An Overview

The wave age ξ is defined as the ratio of the phase velocity C_0 of waves corresponding to the spectral peak frequency ω_0 to the mean wind above the sea level (e.g., at 10 m height):

$$\xi = C_0/U = g/U\omega_0 \tag{1}$$

The data presented in section 3 cover a broad range of sea development stages from that of moderate degree, $\xi \sim O(1)$, to a very well developed sea, $\xi \gg 1$. This range can be treated in the framework of the weak turbulence theory (WTT) for surface gravity waves [*Zakharov and Filonenko*, 1966; *Zakharov and Zaslavskii*, 1982, 1983], which accounts for wave-wave interaction in resonant wave tetrads [*Hasselmann*, 1962]. Let us summarize a few relevant concepts which facilitate the interpretation of the data.

For a statistically stationary and spatially homogeneous wave field, WTT predicts two possible regimes of wave energy and action flow through the spectrum: the direct inertial cascade, in which the wave energy flux Q is conserved, and the inverse cascade, in which the wave action flux P is conserved [*Zakharov and Filonenko*, 1966; *Zakharov and Zaslavskii*, 1982] while the energy flux is zero. In the course of the wave field's evolution, the inverse cascade of the wave action is accompanied by a nonconservative flow of energy to low wavenumbers [*Hasselmann*, 1962; *Hasselmann et al.*, 1973]. The inverse cascade causes a gradual decrease of the spectral peak wavenumber k_0 with an increasing wind fetch (distance along the wind vector) and duration (time from the start of the wind). Thus at a given wind U, the nondimensional spectral peak frequency $\tilde{\omega}_0 = U\omega_0/g$ represents a measure of wave development. In the present work, we consider only the cases with an infinite wind duration. Hence the degree of sea development depends only on the wind fetch, and the wave field is spatially inhomogeneous. Kolmogorov-type spectra can still be used in this situation for crude estimates, as was demonstrated by *Zakharov and Zaslavskii* [1983] and *Glazman and Srokosz* [1991], although certain refinements, as discussed in the following sections, are necessary.

For moderately developed waves ($\xi \leq 1$), the relative extent of the wavenumber subrange corresponding to the inverse cascade is negligible in comparison with that of the direct cascade. Then the "equilibrium" range in the (energy) spectrum is dominated by [*Zakharov and Filonenko*, 1966]

$$F(k) = \alpha_q g^{-1/2} Q^{1/3} k^{-7/2} \qquad S(\omega) = 2\alpha_q g Q^{1/3} \omega^{-4} \tag{2}$$

where $F(k)$ is the wavenumber spectrum and $S(\omega)$ is the frequency spectrum. The ω^{-4} equilibrium range was also discovered by *Toba* [1973] on the basis of field observations. The nondimensional constant α_q plays a role similar to that of the Kolmogorov constant in turbulence. Q is the spectral flux of energy toward high wavenumbers. In a statistically anisotropic wave field, the two-dimensional wavenumber spectrum includes an angular distribution factor $\Upsilon_k(\theta)$, which is assumed here to be normalized to yield unity upon integration over all angles θ. Although we shall omit this factor in the subsequent equations, its significance will be discussed in sections 5 and 7. The rate Q of the energy transfer down the spectrum is given in terms of the energy flux per unit surface area and per unit mass of water. Earlier it was shown [*Phillips*, 1985; *Glazman*, 1992] that Q does not have to be constant in frequency in order to yield power law $S(\omega) \sim \omega^{-4}$. Actually, Q is a slowly growing function of k, consistent with the Miles mechanism of wave generation.

At high degrees of wave development ($\xi \gg 1$), when the inverse cascade range has become broad in comparison with the direct cascade range, the spectrum is controlled primarily by two factors: the wave action cascade toward low wavenumbers and, as discussed in sections 5 and 6, the advective energy transfer in a spatially inhomogeneous wave field due to the wave group velocity. If the latter is discarded, a simplified theory [*Zakharov and Zaslavskii*, 1982] assuming a spatially homogeneous wave field yields a Kolmogorov spectrum determined by the inverse conservative cascade of wave action:

$$F(k) = \alpha_p P^{1/3} k^{-10/3} \tag{3}$$

This corresponds to $S(\omega) \sim \omega^{-11/3}$.

One can further idealize the situation by assuming that the wind energy input is concentrated at wavenumbers (the "generation range") separating the two inertial subranges.

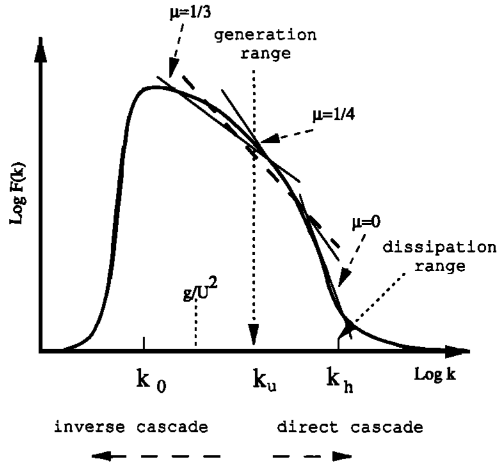

Figure 1. Wavenumber subranges in an equilibrium spectrum of developed seas. Thin solid straight lines represent power law approximations, in the form $k^{-4+2\mu}$, for the specific wavenumber subranges: μ decreases with an increasing distance away from the spectral peak wavenumber k_0. The thick-dashed line represents a power law approximation for the entire equilibrium range: the "effective value" of μ is determined by the relative extent of the constituent subranges.

As is discussed in the following sections, the forms (2) and (3) are not very useful, for we do not know in advance how the input fluxes, Q_u and P_u, are related to the inertial fluxes Q and P through the spectrum. On dimensional grounds, P and Q can be expressed in terms of the mean wind speed U as

$$P \propto g^{-2}U^4 \qquad Q \propto U^3 \tag{4}$$

Then the entire equilibrium range can be presented in the form

$$\begin{aligned} F(k) &= \beta(U^2/g)^{2\mu}k^{-4+2\mu} \\ S(\omega) &= 2\beta g^2(U/g)^{4\mu}\omega^{-5+4\mu} \end{aligned} \tag{5}$$

which reduces to (2) or (3) by setting $\mu = 1/4$ or $\mu = 1/3$ for $\xi \leq 1$ and $\xi \gg 1$, respectively. Furthermore, β is the generalized Phillips constant whose value can be expressed in terms of the Kolmogorov constants. In general, μ is a slowly decreasing function of the wavenumber [*Glazman et al.*, 1988; *Glazman and Weichman*, 1989; *Glazman and Srokosz*, 1991]: $\mu = \mu(k)$ (Figure 1). Its maximum lies in the subrange associated with the inverse cascade. At frequencies above the generation range, μ passes through 1/4 and reaches zero in the Phillips "saturation" range [*Phillips*, 1977] (if the energy input is sufficiently high for such a range to occur). In the Phillips range the spectrum tends to

$$F(k) = \beta k^{-4} \tag{6}$$

This corresponds to a non-Gaussian field of the surface height variation characterized by cusped wave crests. WTT is not applicable to the strongly nonlinear waves described by (6). The drop of μ below 1/4 (i.e., from weak turbulence to stronger nonlinearity) can be described on the basis of a heuristic theory of multiwave interactions [*Glazman*, 1992].

Experimentalists usually report an overall apparent value of the exponent and a wave-age-dependent value of the Phillips constant β in the power laws (5). This "effective" exponent yields an apparent fractal (Hausdorff) dimension of the surface: $D_H = 2 + \mu$ [*Glazman and Weichman*, 1989]. Being a function of the relative extent of the idealized subranges (2), (3), and (6), the apparent "codimension" μ is determined by the wave age. Theoretical dependencies for the effective μ and β as functions of ξ are presented in section 4.

The low-wavenumber cutoff (the "outer scale" of the spectrum) is steep and can be approximated by a smeared unit step function $H(k/k_0 - 1)$. A commonly accepted form of $H(\ )$ is given by $\exp[-(k/k_0)^{-2}]$—as follows from the empirical P-M spectrum. Thus the energy-containing range is approximated by

$$F(k) = \beta(U^2/g)^{2\mu}k^{-4+2\mu}\exp[-(k/k_0)^{-2}] \tag{7}$$

Using the dispersion relation for gravity waves, the low-frequency cutoff is related to the wave age (equation (1)) by

$$k_0 = (g/U^2)\xi^{-2} \tag{8}$$

Typical values of ξ for open ocean waves lie in the range 1.5–3 [*Glazman and Pilorz*, 1990]. The limiting wave age for the "fully developed" sea still remains unknown, and the existence of the FDS state hypothesized by *Kitaigorodskii* [1962, 1970] has been questioned on both theoretical and experimental grounds [*Glazman*, 1991b] along with the empirical P-M spectrum which claims to represent FDS [*Pierson*, 1991].

Analyzing the spatial evolution of stationary wave fields, we shall examine in sections 5 and 6 the well-known empirical relationships between the wave age, the nondimensional wind fetch $\tilde{x}$ ($\tilde{x} = gx/U^2$, where x is the dimensional fetch), and the nondimensional wave energy, e:

$$\xi = Ae^a \tag{9}$$

$$e = B\tilde{x}^b \tag{10}$$

$$\xi = C\tilde{x}^c \tag{11}$$

Sometimes these are called fetch laws. Of particular interest are variations in the values of A, B, C, a, b, and c revealed by comparing reports of different experimentalists. The dimensionless wave energy (called alternatively the generalized nondimensional fetch [*Glazman*, 1991b]) is defined as

$$e = \frac{\int F(\mathbf{k})\,d\mathbf{k}}{(U^2/g)^2} \equiv \frac{\int S(\omega)\,d\omega}{(U^2/g)^2} \tag{12}$$

Since only two of the three equations (9)–(11) are independent, we shall consider only (9) and (11). Experimental data on the parameters of the fetch laws are summarized in Table 1. Conditions characterizing individual experimental setups are highly diverse. As is explained in section 5, the differences in atmospheric boundary layer stratification, in the range of the wind speed and fetch values covered, and in other factors including local depth and hydrography have effects on the parameters reported in Table 1.

Fetch laws (9)–(11) also follow from the action and energy transfer equations [*Zakharov and Zaslavskii*, 1983; *Glazman and Srokosz*, 1991]. The derivation involves certain simpli-

Table 1. Field Observations

Data Source	$\xi = Ae^a$		$e = B\bar{X}^b$		$\xi = C\bar{X}^c$	
	A	a	$B \times 10^{-7}$	b	C	c
Dobson	5.62	0.29	12.7	0.75	0.094	0.24
JONSWAP	7.94	0.33	1.6	1.0	0.045	0.33
Donelan	5.98	0.30	8.4	0.76	0.086	0.23
Phillips			1.6	1.0	0.089	0.25
Ross			1.2	1.1	0.084	0.27
Walsh			1.9	1.0	0.069	0.29
Kahma					0.050	0.33
Mitsuyasu			2.89	1.0	0.051	0.33
Glazman	7.65	0.31				

Abbreviations of data sources are as follows: Dobson, *Dobson et al.* [1989]; JONSWAP (Joint North Sea Wave Project), *Hasselmann et al.* [1973]; Donelan, *Donelan et al.* [1985]; Phillips, *Phillips* [1977], Ross, *Ross* [1978] and *Liu and Ross* [1980]; Walsh, *Walsh et al.* [1989]; Kahma, *Kahma* [1981]; Mitsuyasu, *Mitsuyasu et al.* [1971]; Glazman, *Glazman* [1991a].

fying assumptions regarding the wind input in a developed sea state. By a developed sea we understand a wave field having a broad wavenumber spectrum, such that a short-range asymptotic of the structure function $D(\mathbf{r}) \equiv \langle[\zeta(\mathbf{x}+\mathbf{r}) - \zeta(\mathbf{x})]^2\rangle$ for the surface elevation field $\zeta(\mathbf{x})$ due to gravity waves reduces to [*Glazman and Weichman*, 1989]

$$D(r, \Theta) \approx L^{2\mu}(\mu, \Theta) r^{2-2\mu} \tag{13}$$

where the dimensional coefficient L (called the "topothesy") is independent of the spectral peak wavenumber k_0: $L^{2\mu} = \beta(U^2/g)^{2\mu} f(\mu, \Theta)$. Since $D(r, \Theta)$ is evaluated for small spatial lags r, (13) pertains to the high-wavenumber range of the gravity wave spectrum dominated by the direct energy cascade. In particular, one can use $\mu = 1/4$ and express β in terms of the Kolmogorov constant α_q. In general, (13) is valid if [*Glazman and Weichman*, 1989].

$$(k_0 r/2)^{2\mu} \ll \mu\Gamma(\mu)/(1-\mu)^2\Gamma(1-\mu) \tag{14}$$

Under this condition, the field $\zeta(\mathbf{x})$ exhibits "fractal geometry" characterized by a pattern of continuously "nested" wavelets of a monotonically decreasing size. The wave slope variance, estimated as $\gamma^2 \approx D(\lambda)/\lambda^2$, where λ is the relevant (short) spatial scale of interest, becomes independent of the dominant wavelength $2\pi/k_0$. As a result, neither wind fetch nor wave age can appreciably influence γ^2. Owing to the exclusive role of the wave slope for the induced air pressure and shear stress fields [*Phillips*, 1977, chapter 4.2], we anticipate the wind-wave coupling to be independent of the wind fetch. Hence in a developed sea, the mean wind U becomes the only external parameter of the wind input, and at scales satisfying (14) we assume a universal regime of air-sea interactions.

The wind input may be envisioned as occurring in the fashion of the Miles mechanism, i.e., being proportional to $F(\mathbf{k})$ and attaining its spectral maximum at wavenumbers above g/U^2. The integral fluxes of wave action and energy take the form

$$P_u = \int p^+(\mathbf{k})\, d\mathbf{k} = \varepsilon R_p^+ g^{-2} U^4 \tag{15}$$

$$Q_u = \int q^+(\mathbf{k})\, d\mathbf{k} = \varepsilon R_q^+ U^3 \tag{16}$$

where $p^+(\mathbf{k})$ is the spectral density of the action input flux (per unit surface area and per unit mass of water), $q^+(\mathbf{k})$ is the spectral density of the energy flux, and ε is the ratio of air and water densities. Both $p^+(\mathbf{k})$ and $q^+(\mathbf{k})$ are confined to the high-wavenumber range. In the wave-modeling literature, these are called the wind source functions. For a developed sea, the bulk transfer coefficients, R_p^+ and R_q^+, are assumed to be independent of the wind fetch. If, however, one considers a broad range of sea development stages, as is covered in Table 1, the assumption of constant R_p^+ and R_q^+ has to be relaxed to allow for a (relatively weak) dependence of these "constants" on the nondimensional fetch. Accounting for wind-wave interaction at lower frequencies (e.g., for the feedback flux of momentum from fast moving long waves to the atmosphere) would also result in a dependence of R_p^+ and R_q^+ on additional parameters.

3. Buoy Observations of Developed Seas at Equilibrium With a Steady Wind

The present empirical knowledge on the wave field evolution is based largely on observations at limited wind fetches and relatively small depths, conditions encountered in the Great Lakes, North Sea, and other closed or semiclosed basins convenient for field experiments [e.g., *Toba*, 1973; *Donelan et al.*, 1985; *Dobson et al.*, 1989]. These observations consistently show $\mu \approx 1/4$ and support the FDS concept with the limiting wave age ξ_{FDS} about 1.2. The cases characterized by much greater values of the wave age are usually discarded as allegedly irrelevant to wind-driven seas. For example, in their study of fully developed seas, *Ewing and Laing* [1987] used quantitative criteria to eliminate from their data set all observations contradictory to the FDS concept and to the P-M spectrum. For instance, one of their tests required that the wave age not exceed 1.45. Observations in open ocean regions with stable winds and large wind fetches are relatively rare and report $\xi \gg \xi_{FDS}$ [*Glazman*

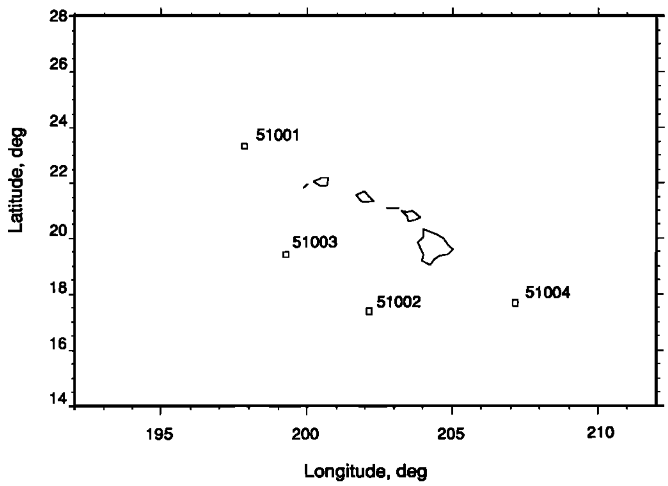

Figure 2. Locations of main (Hawaiian) NDBC buoys used in the data set.

and Pilorz, 1990; *Glazman*, 1991a] and a different power law $S(\omega) \sim \omega^{-p}$, where p can reach 3 [*Grose et al.*, 1972].

We examined a 2-year series of wind and wave observations by autonomous NOAA buoys operated by the National Data Buoy Center (NDBC). Most of the observations selected for our data set are from the Pacific trade wind zone near the Hawaiian Islands (Figure 2). This region is characterized by large values of wind fetch and duration. A number of observations were added also from NDBC buoys in the North Atlantic to cover cases of moderate sea states with ξ near 1.

Only the buoys of the Nomad type were used. These buoys' hulls are boat shaped, 6 m long, and 3 m wide. The accuracy of spectrum measurements by these buoys was estimated by *Murphy* [1979], who derived a reliable hull power transfer function and found that at frequencies up to 0.36 Hz the relative error, $\Delta S(f)/S(f)$, does exceed 9.4% while the average error for the frequency range from 0.12 to 0.5 Hz is only 4.2 percent.

The anemometer height is 5 m. Assuming neutral stratification of the marine boundary layer, we referenced the mean wind to a standard height of 10 m. (Accounting for actual stratification would yield only an insignificant correction to the mean wind U.) The mean wind represents an 8.5-min average. The size of the buoys as well as the accuracy of spectral estimates allowed us to analyze the range of wave frequencies f_i from 0.03 Hz to 0.35 Hz with the Δf step of 0.01 Hz. Since the buoys provide only the frequency spectra, the directional properties of the wave field remained beyond the scope of the present work. The buoys report data on an hourly basis, with a few exceptions when the interval is 3 hours.

Our consideration was limited to steady wave fields at equilibrium with the observed statistically stationary wind. The data set was prepared by browsing through thousands of continuous wave and wind observations in order to discard cases in which the dominance of a given wind as the main factor determining the observed spectrum could be questioned. With practically no limitations on the length of the (hourly) records, we were able to check time histories for wind speed and direction, wave spectra, and wave age, as illustrated in Figures 3–5. The cases with appreciable linear trends and, generally, all cases with relative variations of wind speed in excess of 15% of the mean values (calculated for each 6-hour interval) were eliminated. The wind direction was required to remain within plus or minus 15° of the mean direction. Also we eliminated cases in which wave spectra showed appreciable temporal evolution (third panel from the top in Figures 3–5). A few typical cases in which wave spectra were classified as stationary (Figures 3 and 4) or nonstationary (Figure 5) are illustrated. Finally, we ensured that the wave field contained no significant swell. By swell we understand a wave system generated in a remote location by a wind field whose speed and direction are noticeably different from the local wind. To eliminate such cases, we checked the shape of wave spectra for occurrences of multiple peaks and other conspicuous features identifying mixed seas. This procedure proved successful in an earlier study by *Glazman and Pilorz* [1990], to which the reader is referred for details and additional illustrations. The total number of "ideal" steady state cases retained for the subsequent analysis was 629.

The data employed in this analysis did not permit checking the degree of spatial inhomogeneity in the wind field. Therefore our data set is likely to contain some cases in which a local wind speed upwind of the buoy location may be considerably lower or higher than that observed at the buoy. Such variations should contribute to the scatter of experimental points in Figure 8 and complicate data interpretation. However, the wind's spatial inhomogeneity represents an intrinsic property of wind fields and is encountered in any field observations. Therefore the notion of the wind fetch may have to be revised to account for (at least some type of) the wind field's spatial inhomogeneity. This issue is discussed further by *Glazman* [1991b].

The wave age ξ was estimated using the spectral peak frequency f_0 and mean wind U. The effective fractal codimension μ and the generalized Phillips constant β were derived from the observed spectra $S(f)$ as follows. We integrated $S(f)$ and $f^{-1}S(f)$ numerically from a certain $f_{\min} > f_0$ to the high-frequency cutoff $f_{\max} = 0.35$ Hz to obtain estimates of wave energy E and action N for this "equilibrium" range. Requiring that E and N coincide with the energy and action obtained by integrating the analytical wave spectrum (equation (5)) yields two equations for μ and β:

$$\begin{aligned} 2\beta' g^2 (U/g)^{4\mu} \int_{f_{\min}}^{f_{\max}} f^{-5+4\mu}\, df &= E \\ 2\beta' g^2 (U/g)^{4\mu} \int_{f_{\min}}^{f_{\max}} f^{-6+4\mu}\, df &= N \end{aligned} \tag{17}$$

The prime in β' distinguishes this quantity from β appearing in (5) and (7), where angular frequency ω is used. Equations (17) have been solved by iterations considering $f_{\min}/f_{\max}$ as a small parameter. Only the cases with $f_{\min}/f_{\max} \leq 0.7$ were used in these calculations, and only the spectra containing at least 10 frequency points within the selected range were considered. The relationship between β' and β is

$$\beta = (2\pi)^{4(1-\mu)} \beta' \tag{18}$$

The integration limit $f_{\min}$ must lie sufficiently above the spectral peak frequency f_0 in order to obtain μ representa-

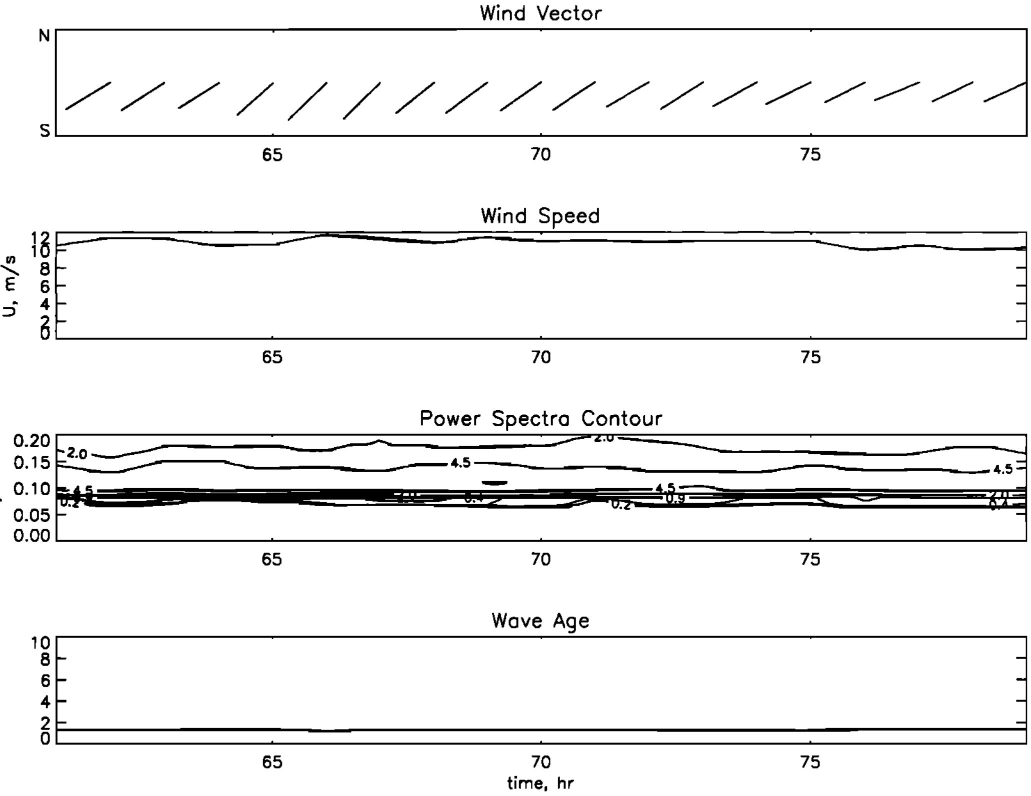

Figure 3. Time history of wind vector, wave spectrum, and wave age observed at buoy 51002, illustrating a steady state wave field at equilibrium with a given wind. Top to bottom: wind vector, wind speed in meters per second, contour plot of the wave frequency spectrum evolving in time, and wave age estimated using (1) where U and ω_0 are based on hourly buoy reports. The total number of cases taken from this record is 15.

tive of the "equilibrium range." Practically, we selected $f_{\min}$ to be a multiple of f_0: $f_{\min} = 1.5 f_0$. It was found that in the logarithmic coordinates, the typical shape of wave spectra in the given range $f_{\min}, f_{\max}$ is convex, i.e., $d^2(\log S)/d(\log f)^2 < 0$. Figure 6 illustrates a few typical cases. An interpretation of this observation is offered in section 4.

A more traditional way of estimating the spectral exponent and the Phillips constant is to plot the observed spectrum in logarithmic coordinates and then fit a straight line to all the points within the selected frequency range. Unfortunately, this procedure does not guarantee correct values of E and N. Besides, the μ and β so derived are sensitive to the high-frequency range of the wave spectra which may be affected by the buoy hull characteristics. In Figure 7 we illustrate the agreement between the observed spectra and the fitted power law forms.

In Figures 8 and 9, μ and β obtained using (17) and (18) are plotted versus wave age. The plots show that ξ can exceed 3, which is well above the limit for the fully developed sea. Evidently, a wave age greater than 2 is a typical feature of open ocean waves. Furthermore, the plots exhibit a monotonic growth of μ as the wave age increases, tending to about 0.5 at sufficiently large ξ. As is suggested in sections 5 and 6, such large values of μ (noticed first by *Grose et al.* [1972]) are associated with the advection of the wave energy in a spatially inhomogeneous wave field.

The 0.35-Hz frequency cutoff and the prevalence of well-developed sea states in our data set do not permit obtaining reliable trends for μ and β at small values of the wave age, i.e., at $\xi \le 1$. Furthermore, the high values of ξ and μ in Figures 8 and 9 may not be the largest possible in an open ocean. When preparing our "ideal" data set, we may have unjustifiably eliminated some legitimate cases with particularly large ξ. Indeed, our requirements on the wind history were very rigid. However, this conservative choice reduces the well-known conceptual difficulty regarding the separation of swell from a wind-driven sea.

4. The Shape of the Wave Spectrum

The observed trends in μ and β provide important clues regarding the energy balance. To better understand the connection we shall first derive the trends theoretically on the basis of the results of WTT for an isotropic wave field.

As was suggested earlier [*Glazman and Srokosz*, 1991], one can approximate the actual spectrum $F(k)$ characterized by a gradually decreasing value of μ by a composite spectrum, $F_c(k)$:

$$F_c(k) = \beta_p (U^2/g)^{2/3} k^{-10/3} \exp[-(k/k_0)^2] \qquad 0 < k \le k_u$$
$$F_c(k) = \beta_q (U^2/g)^{1/2} k^{-7/2} \qquad k_u < k < \infty \tag{19}$$

The two equations (19) correspond to two basic regimes of the energy and action flow, as was mentioned in section 2. Here, $\beta_{q,p}$ are universal constants which can be expressed in terms of the Kolmogorov constants (they play only an

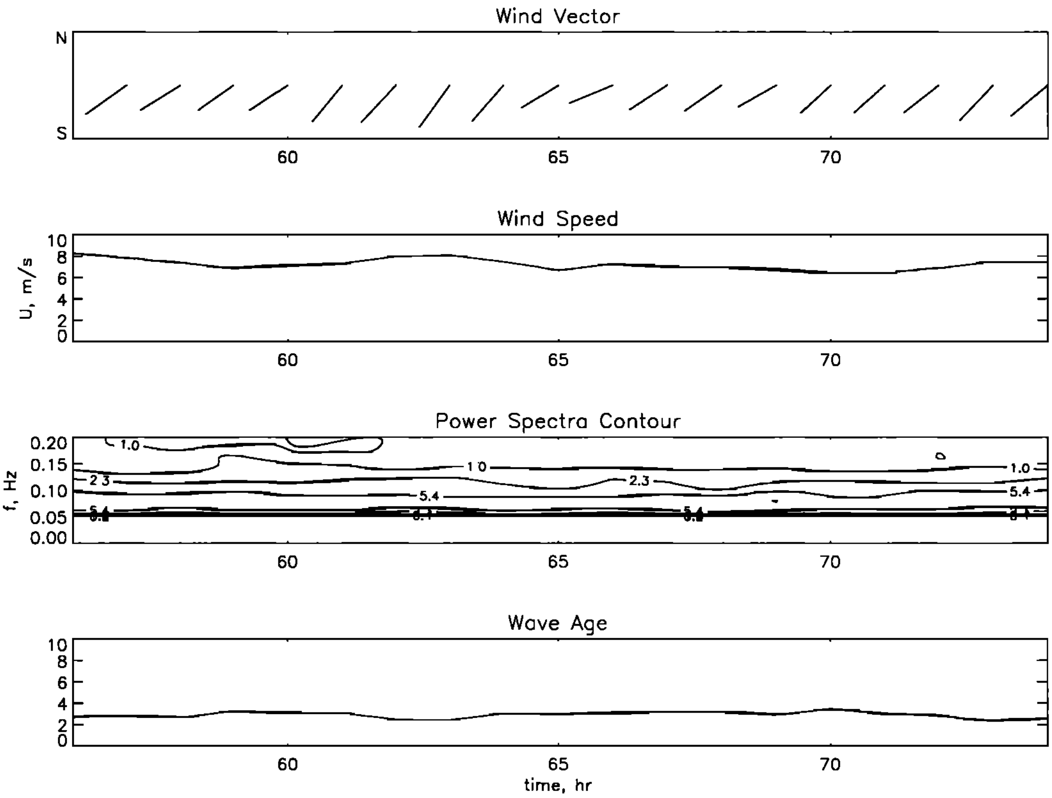

Figure 4. The same as Figure 3, for buoy 51001. The total number of cases taken from this record is 9.

intermediate role in this derivation). The spectral peak wavenumber k_0 is given by (8), and the spectral maximum in the energy flux from wind to waves is assumed to occur at

$$k_u = (g/U^2)\eta^{-2} \tag{20}$$

where $\eta^{-2} > 1$ is a constant. Equation (20) is a simple consequence of the Miles theory which yields the spectral density of the energy flux from wind to waves being linearly proportional to the wave spectrum: $q(\omega) \propto \omega\phi(\Omega)S(\omega)$. Here, $\Omega = \omega/\omega_U$, $\omega_U = g/U$, and ϕ can be presented as $\phi(\Omega) = H(\Omega - 1)(\Omega - 1)^n$ where $n = 1$ in the case of the *Snyder et al.* [1981] parametrization, $n = 2$ in the case of *Hsiao and Shemdin* [1983] and other authors' parametrizations (see Appendix B) and $H(\ )$ is a (smeared) unit step function which expresses the shadowing effect (waves moving faster than the wind do not receive energy from wind): $H \approx 0$ for $\Omega < 1$ and $H \approx 1$ for $\Omega \geq 1$. As a result, for the "energy generation range" (i.e., for $\Omega \gg 1$), one finds (omitting all constants that are not important for this discussion): $q(\omega) \propto \omega^{-4+4\mu}(\omega/\omega_U - 1)^n$. Obviously, the frequency at which this function attains its maximum is independent of ω_0 and is linearly proportional to ω_U. In the wavenumber domain, this is expressed by (20) in which the "correction factor" η^{-2} is actually about 2.

The requirement that the two branches of (19) meet at $k = k_u$ yields a relationship between the universal constants:

$$\beta_p = \beta_q \eta^{1/3} \tag{21}$$

Since the actual spectral shape (7) with $\mu = \mu(k/k_0)$ is not known, and because the experimental data provide only the overall, effective exponent, we shall again estimate the apparent μ for the entire equilibrium range. A requirement that the composite spectrum (19) yield the same integrated energy and action as would follow from (7) with a constant μ yields two equations for μ and β:

$$B\Gamma(1 - \mu)\xi^{4(1-\mu)} = \Gamma(2/3,\ \tau)\xi^{8/3}\eta^{1/3} + (4/3)\eta^3 \tag{22}$$

$$B\Gamma(5/4 - \mu)\xi^{5(1-\mu)} = \Gamma(11/12,\ \tau)\xi^{11/3}\eta^{1/3} + \eta^4 \tag{23}$$

where

$$B = \beta(\xi)/\beta_q \qquad \tau = (\eta/\xi)^2 \tag{24}$$

Here $\Gamma(a,\ b)$ is the incomplete gamma function. In the derivation of (23) we used the dispersion relation $\omega = (kg)^{1/2}$ to eliminate ω from the spectral density of the wave action, $N(k) = F(k)/\omega$. The system (22) and (23) has a simple solution, B and μ, derived in Appendix A.

Functions $B(\xi)$ and $\mu(\xi)$ are plotted in Figure 10 for several values of η. In Figure 11 we plot the result for the value $\eta = 0.75$, which agrees best with the trends observed in Figures 8 and 9. Apparently, at ξ near 1, $B(\xi)$ can be approximated (through a least squares fit) by a power law

$$B(\xi) \approx S\xi^{-s} \tag{25}$$

which allows one to compare the theoretical prediction with the empirical data of *Donelan et al.* [1985]. As can be seen from Figure 11, the agreement is quite good. Finally, we should emphasize that the wave-age-dependent β and μ should be viewed as ad hoc parameters, a consequence of a decrease in the actual value of $\mu(k/k_0)$ with an increasing distance from the spectral peak.

Apparently, within the appropriate range of the wave age values, the predicted trends are in reasonable agreement

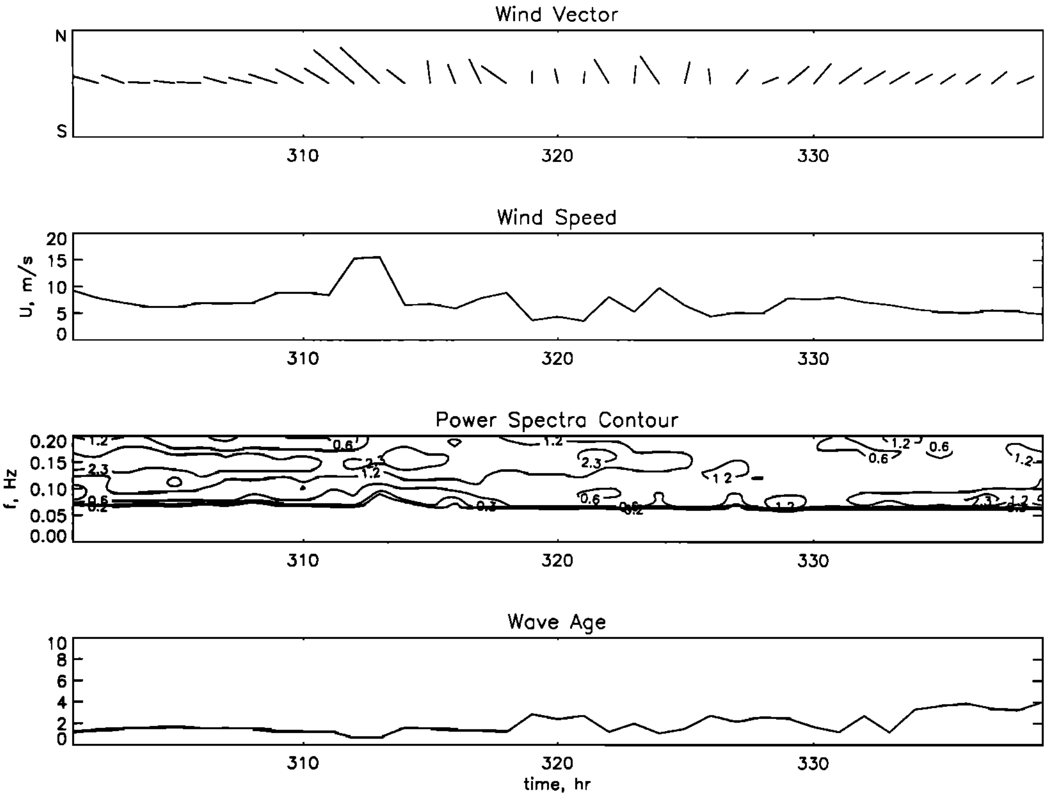

Figure 5. Example of an unsteady sea state. See caption for Figure 3.

with the observations in Figures 8 and 9, while at too small and too large ξ these WTT-based predictions disagree with the observations. At low ξ the value of μ approaching zero can be explained by incorporating the Phillips range (equation (6)) into the composite spectrum model. A dynamical model describing the transition from the weak turbulence regime to a regime of stronger nonlinear wave-wave interactions is offered by *Glazman* [1992]. The large values of μ approaching 1/2 at $\xi \gg 1$ are interpreted in the next two sections, along with their implications for air-sea interactions.

5. Spatially Inhomogeneous Wave Field

Conservation of the wave action flux in the inverse cascade is consistent with the traditional understanding of the local wind-wave equilibrium as attained as a result of energy

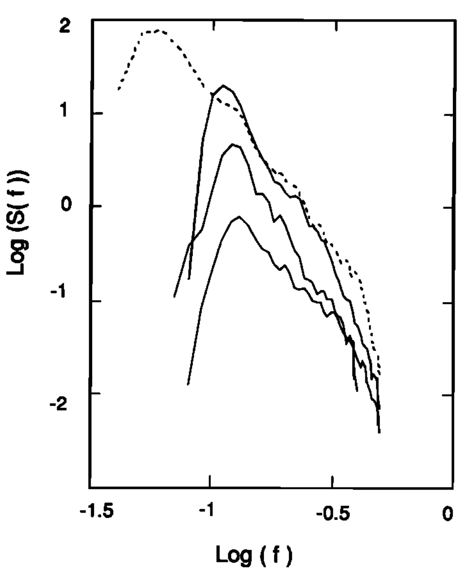

Figure 6. Typical shapes of statistically stationary wave spectra $S(f)$ observed near the Hawaiian Islands.

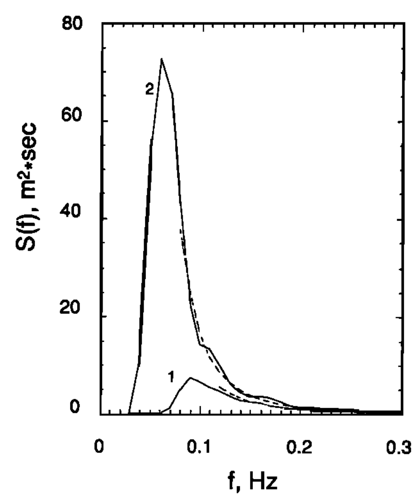

Figure 7. Empirical fit to the equilibrium range of wave spectra in the form of (5) for which the effective values of μ and β are calculated using (17). Solid curves are the observed wave spectra at wind speed 9 m/s and wave age 1.9 (curve 1) and at wind speed 12 m/s and wave age 2.2 (curve 2). The dashed curves are the empirical fit (equation (5)).

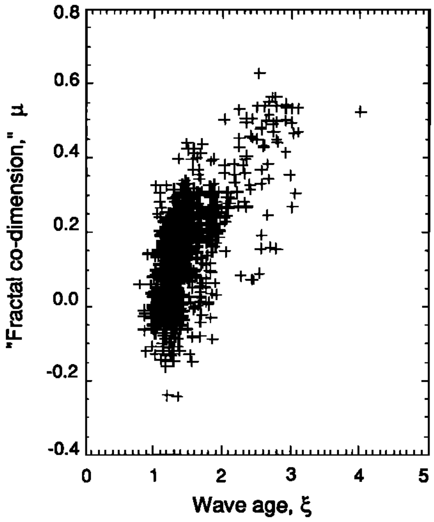

Figure 8. The apparent "fractal codimension" μ versus wave age ξ calculated from (17) and (18) for 629 spectra.

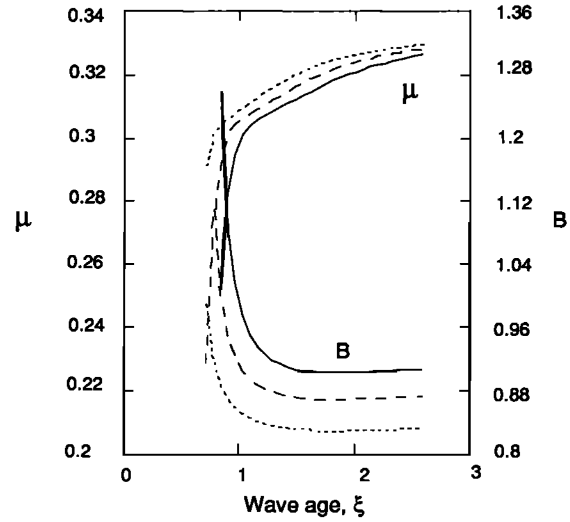

Figure 10. Analytical solution of (22) and (23) for three values of η. Solid curves, $\eta = 0.7$; short-dashed curves, $\eta = 0.9$; long-dashed curves, $\eta = 0.8$.

dissipation at high wavenumbers. Indeed, according to the model of *Zakharov and Zaslavskii* [1982, 1983] (hereinafter referred to as Z-Z), the inverse energy cascade is zero; hence the entire energy flux from wind goes toward high wavenumbers. (General discussion on the direction of spectral fluxes is given in chapter 3 of *Zakharov et al.* [1992].) In what follows we show that for a developed sea state, such a simple and attractive picture is inconsistent with both the observed wave spectra and the observed wave field evolution: the large values of μ and the high values of A, a, and c in the fetch laws (9)–(11) reported in Table 1 point to a nonconservative spectral flux of wave action accompanied by a considerable leak of energy to the low-wavenumber range.

The Z-Z model for the spatial evolution of a wave field provided the first theoretical explanation of the power law (11). The spatial evolution of a statistically stationary wave field is due to an intrinsic anisotropy of wave spectra. It is well known that the two-dimensional wave spectra $F(\mathbf{k})$ are characterized by a rather narrow angular distribution with the dominant wave propagation in the direction of the mean wind. Apparently, a preferential direction of wave propagation should result in an advective flow of the wave energy and action. The transfer of the wave action spectral density, $N = F(\mathbf{k})/\omega$, is described by

$$\nabla \cdot (\mathbf{c}_g N) + \nabla_k \cdot T(\mathbf{k}) = p \tag{26}$$

where $\mathbf{c}_g = \partial\omega/\partial\mathbf{k}$, $\nabla_k \cdot T(\mathbf{k})$ is the interaction (collision) integral for gravity waves, and p is the source function for the spectral density of the wind input. Z-Z assumed that the advective term in the left-hand side has no appreciable effect on the shape of the wave spectrum, except for the value of k_0. In other words, at $k > k_0$ the wave action flux is

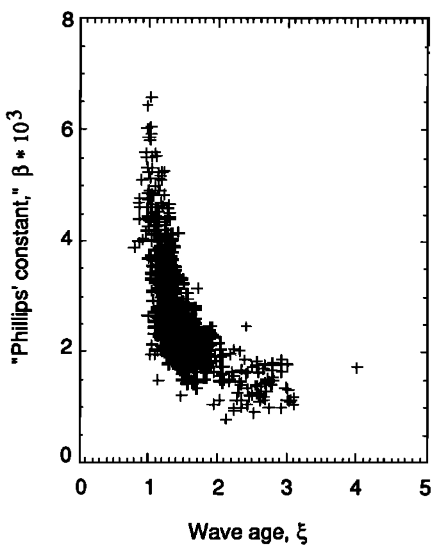

Figure 9. The "generalized Phillips constant" β versus wave age ξ calculated from (17) and (18).

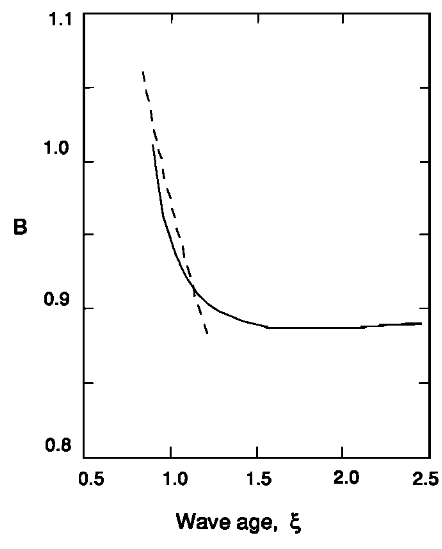

Figure 11. Solution of (22) and (23) at $\eta = 0.75$ for $B(\xi)$. The dashed curve is a regression curve approximating $B(\xi)$ by (25) for a range of ξ from 0.9 to 1.2. This empirical fit, characterized by $s \approx 0.5$, agrees with *Donelan et al.*'s [1985] $s \approx 0.55$.

conserved: $\int \nabla_k \cdot T(\mathbf{k})\, d\mathbf{k} = 0$ and equation (3) remains approximately valid for most of the wavenumber range. Then integrating (26) over all wavenumbers yields a crude model for the wave field spatial evolution

$$\nabla \cdot \int \mathbf{c}_g N \, d\mathbf{k} = P_u \tag{27}$$

where $P_u \equiv \int p \, d\mathbf{k}$ is the total input flux, which is cascaded toward low wavenumbers. Assuming no variations normal to the wind vector, the spatial evolution occurs only along the fetch x. Then substituting (7) with $\mu = 1/3$ into (27) yields an equation for the spectral peak wavenumber:

$$\frac{\partial}{\partial x}\left(\frac{\alpha_p P_u^{1/3}}{2} \int_0^\infty k^{-10/3} \exp\left[-(k_0/k)^2\right] dk\right) = P_u \tag{28}$$

For a developed sea state, in which (14) holds, P_u depends only on the mean wind:

$$P_u = \varepsilon R_p g^{-2} U^4 \tag{29}$$

where ε is the ratio of the air and water densities and R_p is the (constant) bulk coefficient of action transfer from wind to waves. Equation (29) can be obtained not only on dimensional grounds but also from a spectral model of wind input as shown in Appendix B. The nondimensional wind fetch is defined as

$$\bar{x} = gx/U^2 \tag{30}$$

Using (8) and (29), an exact solution of (28) takes the form of equation (11) with [*Zakharov and Zaslavskii*, 1983]

$$c = 3/14 \qquad C = [4(\varepsilon R_p)^{2/3}/\alpha_p \Gamma(7/6)]^{3/14} \tag{31}$$

Expressions (9) and (10) for the nondimensional wave energy e are derived by substituting (7) with $\mu = 1/3$ into the integral (12) and using (11) and (31). Thus we arrive at

$$a = 3/8 \qquad A = [\alpha_p(\varepsilon R_p)^{1/3}\Gamma(2/3)/2]^{-a} \tag{32}$$

Comparing the exponents a and c with the data in Table 1 we find appreciable discrepancy with all experiments. Partly, this is because most of the observations in Table 1 are dominated by cases of moderately developed seas with $\xi \leq 1$. For such cases, the direct energy cascade dominates wave dynamics, and the assumption $\int \nabla_k \cdot T(\mathbf{k})\, d\mathbf{k} = 0$ must be replaced with the corresponding statement for the spectral energy flux: $\int \nabla_k \cdot T(\mathbf{k})\omega \, d\mathbf{k} = 0$. However, an additional, more interesting, source of the discrepancy, as is suggested in the following sections, is due to the fact that the Kolmogorov spectra (2) and (3) ignore the advective transfer of the wave action. Hence they would not be fully appropriate even if the inverse cascade did dominate the wave dynamics.

In the absence of ambient currents and sea level variations, the integrated energy balance, provided that the spectral energy flux in the direct cascade is (approximately) conserved, can be described by [*Glazman and Srokosz*, 1991]

$$\nabla \cdot \int \mathbf{c}_g F(\mathbf{k}, x)\, d\mathbf{k} = \Delta Q \tag{33}$$

where $\Delta Q \equiv \int (q^+ + q^-)\, d\mathbf{k}$ is the net integrated input of the wave energy (wind input minus small-scale dissipation). Assuming ΔQ to be proportional to U^3, one arrives ultimately at

$$\frac{\partial}{\partial x} \frac{\beta}{2} g^{3/2}(U^2/g)^{2\mu} \int_0^\infty k^{-7/2+2\mu} \cdot \exp\left[-(k_0/k)^2\right] dk = \varepsilon R_q U^3 \tag{34}$$

where the general form (7) was used for the wave spectrum, and R_q is the bulk coefficient of the net energy input. For the wind input, the form $\varepsilon R_q^+ U^3$ is confirmed by empirical source functions (as shown in Appendix B), while the breaking wave dissipation term $\int q^-(\mathbf{k})\, d\mathbf{k} \propto U^3$ is justified, for instance, by *Phillips* [1985]. In this formulation the integral energy balance is controlled both by the advective transfer due to the wave group velocity and by the growth of the dominant wavelength with fetch due to nonlinear wave-wave interactions.

Integrating (34) over relatively short segments of x, over which R_q can be assumed constant [*Glazman and Srokosz*, 1991], one finds the solution in the form (11) with

$$c = 1/(5 - 4\mu) \qquad C = [4\varepsilon R_q/\beta\Gamma(5/4 - \mu)]^c \tag{35}$$

Using (7), equations (9) and (12) yield

$$a = 1/(4 - 4\mu) \qquad A = [\beta\Gamma(1 - \mu)/2]^{-a} \tag{36}$$

For $\mu = 1/4$ this is

$$a = 1/3 \qquad A = (0.613\beta)^{-1/3} \tag{37}$$

and equations (35) become

$$c = 1/4 \qquad C = [4\varepsilon R_q/\beta]^{1/4} \tag{38}$$

Evidently, these values are closer to the data of Table 1 than are the values given by (31) and (32).

Variations of the coefficients in Table 1 can be explained on the basis of (35) and (36) as a result of variations in the effective value of μ. In Figures 12 and 13 the data of Table 1 are plotted as points on the planes $\{c, C\}$ and $\{a, A\}$. To compare these with the predicted trends, we also plot functions $C = f_1(c)$ and $A = f_2(a)$ derived from (35) and (36) by eliminating μ. The values of parameters β and R_q that provide the best fit to the experimental points are $\beta \approx 3 \times 10^{-3}$ and $R_q \approx 4 \times 10^{-5}$. While this value of β is in agreement with the data, the coefficient R_q is not known from direct measurements. In Appendix B the present estimate of R_q is shown to be consistent with empirical data on the wind input spectral flux $q^+(\omega)$. The varying μ required for the explanation of the observed trends is associated with a (relatively weak) dependence of μ on ξ as predicted in section 4. Hence the trends found in Table 1 are explained by the fact that different experiments covered different (although overlapping) ranges of the wave age. This was so not only because of the different wind fetch and wind speed ranges covered by different observations but also because of differences in atmospheric boundary layer stratification (in different regions and seasons), which affects the values of R_q and R_p. Indeed, coefficients R_q and R_p can be included in the fetch to highlight their role as a scaling factor in equations (28) and (34).

In conclusion, let us note that the main results (35) and (36) can be further refined. Specifically, one can account for

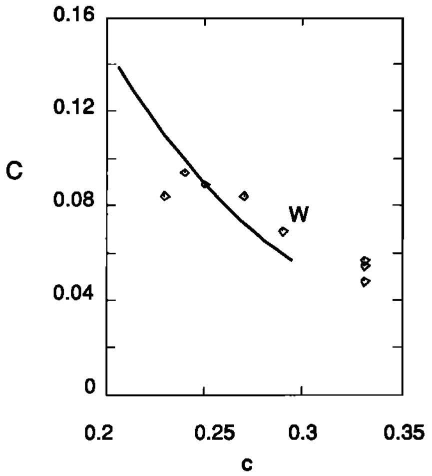

Figure 12. Parameters in equation (11). The solid curve shows C as a function of c obtained by eliminating μ from equations (35). Numerical constants providing the best fit to the data points are $\beta = 3 \times 10^{-3}$, $R_g = 4 \times 10^{-5}$. Diamonds denote experimental data from Table 1. The diamond marked by "W" represents the data of *Walsh et al.* [1989], who claim to have observed the fully developed sea state.

a possible effect of a wave-age-dependent β on the fetch laws' coefficients. Such a correction is relevant only for moderate sea states with ξ near 1. While allowing β to be a function of the wave age (and hence of the wind fetch x) in the left-hand side of (34), we do not have to worry about a corresponding refinement of the wind-wave interaction coefficient in the right-hand side of this equation. Indeed, as is suggested at the end of section 2, the wind input can be treated approximately as being independent of the fetch. According to both the observed and the predicted trends (Figures 9 and 11), the range of ξ in which β experiences most of its variation ends at about $\xi \approx 1.5$. In this regime of moderately developed seas, β can be approximated by a power law (25) where $s \approx 0.5$ and $S \approx 1$. Then, equation (34) yields

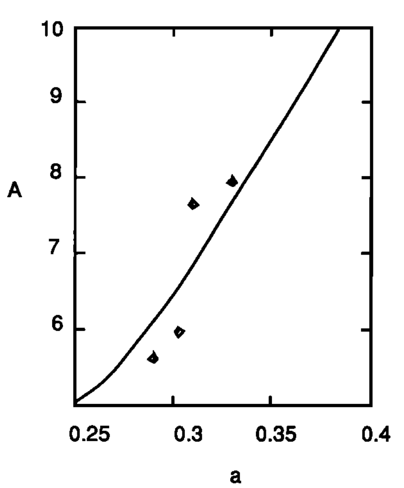

Figure 13. Parameters in equation (9). The solid curve shows A as a function of a obtained by eliminating μ from equations (36). Diamonds denote experimental data from Table 1. See also the caption for Figure 12.

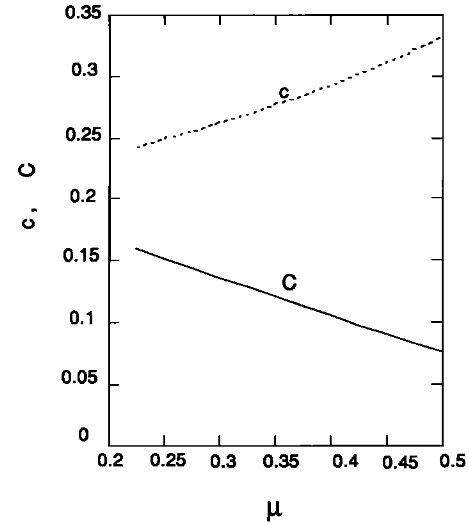

Figure 14. Theoretical dependence of c and C on μ (equation (35)). Note the range of μ.

$$c = 1/(5 - 4\mu - s) \qquad C = [4\varepsilon R_g/\beta_0\Gamma(5/4 - \mu)]^c \tag{39}$$

and in place of (36) we obtain

$$a = 1/(4 - 4\mu - s) \qquad A = [\beta_0\Gamma(1 - \mu)/2]^{-a} \tag{40}$$

6. Effect of Energy and Action Advection on the Spectral Shape

Evidently, the simple theory presented above explains many features of the wave field spatial evolution. However, the assumption that the term $\nabla \cdot (\mathbf{c}_g E)$ in the energy transfer equation (or term $\nabla \cdot (\mathbf{c}_g N)$ in (26)) has no influence on μ is not always justified. Indeed, the values of μ yielding best agreement with the data are generally greater than those obtained with Kolmogorov-type spectra. In Figure 14 we plot c and C, given by (35), versus μ in order to show that the range of μ implicit in Figures 12 and 13 overlaps but does not coincide with that based on the purely inertial spectra (2) and (3). This is also evident from our direct observations (Figure 8). Greater values of μ called for by these comparisons can be explained as follows.

The group velocity term in (26) (and a similar term in the spectral energy balance) describes a loss of wave action (energy) from a given spectral band due to the advective transport. The effect is stronger at lower frequencies for which $\mathbf{c}_g$ is greater. Therefore the lower-frequency spectral components lose wave action (energy) at a faster rate than do the higher-frequency components. This should lead to a flattening of the spectral density function and hence to an increase of the apparent μ. Let us assess the effectiveness of this mechanism.

The characteristic time t_c associated with the action (or energy) advective transfer is found by scaling the advective term in the transfer equation (26). This yields

$$t_c^{-1} \sim \omega/2kx_* \tag{41}$$

where x_* is the characteristic spatial scale of the problem, which we associate with the wind fetch. The characteristic time for the action (or energy) spectral transfer due to nonlinear wave-wave interactions in the resonant wave tetrads is given by [e.g., *Kitaigorodskii*, 1983]

$$t_n^{-1} \sim \omega(ak)^4 \tag{42}$$

where ak is the steepness of the wavelets on the scale k. The ratio

$$t_c/t_n \sim 2(ak)^4 kx_* \tag{43}$$

provides a measure of the relative importance of the nonlinear four-wave resonant interactions as compared to the advective transfer. The wave steepness is higher at high wavenumbers than at low wavenumbers owing to the statistical self-affinity of the wave profiles [*Glazman and Weichman*, 1989]. Hence the dynamics of short gravity waves is strongly affected by the collision integral, while the advective transfer can be disregarded. Provided that x_* is sufficiently large, the advective transfer can be neglected also for longer waves. The wave-wave interaction process is slow for these waves; hence they will receive input from shorter waves (through the inverse cascade) at a very low rate. At wavenumbers of the order of g/U^2, i.e., below the generation range, (43) is estimated as $2\gamma^4\tilde{x}$. Therefore with the characteristic wave slope variance γ^2 of these waves of the order of 10^{-3}, it would take $\tilde{x} \sim 10^6$ to maintain this spectral range at equilibrium with a given wind through the spectral cascade mechanism. This is why such an equilibrium is a highly nonlocal process. At the wavenumbers at which (43) is of the order of unity, the wave spectrum is controlled by both the nonlinear wave-wave interactions and the advective transfer. For this range, the Kolmogorov spectra (2) and (3) become inappropriate.

7. Conclusions

We found that for a wide range of sea development stages, the observed spatial evolution of a stationary wave field can be approximately described by fetch laws (9)–(11) in which the parameters are not constant but vary as functions of sea maturity. Consistent with these variations, the effective exponent, $-p$, for the equilibrium range of the wave spectrum, $S(\omega) \sim \omega^{-p}$, is found to exhibit a growth from -5 to about -3. For a limited range of wave age values, the dependence of p on ξ (expressed in terms of $\mu = \mu(\xi)$) discovered in the experimental data is confirmed by the theoretical predictions based on the energy and action transfer equations. Empirical dependence of the Phillips constant β on the wave age shown in Figure 9 is consistent with the previous findings and (for a limited range of ξ) is also explained in the WTT framework. Simple analytical formulae presented in sections 4 and 5 and the appendices allow one to express parameters of the fetch laws and wave spectrum in terms of "external" factors, such as wind speed, wind fetch, and the energy transfer coefficient C_q. Results of sections 3 and 5 also demonstrate that the dependence of μ and β on ξ is a consequence of artificial approximations of the actual spectrum by a power law with a single exponent. In reality, the spectral "exponent" is a monotonically decreasing function of the wavenumber and frequency. Furthermore, a majority of open ocean observations yield wave age values and spectral exponents that disagree with the "fully developed sea" spectrum. The limiting shape and wave age for well developed seas are still unknown, although we found that wave age values as high as 3 are rather common to open ocean waves at equilibrium with a constant wind. At a large wave age ($\xi \geq 2$), when μ tends to 1/2, the present theoretical understanding of nonlinear wave dynamics is insufficient. Analysis of these results presented in section 6 leads us to the following conclusions.

While WTT (even in its present "naive" form) explains, at least qualitatively, many phenomena of wind-generated waves, a number of important issues remain open. These include the limiting shape of the wave spectrum as the fetch tends to infinity and the relationship between the angular width of the spectrum and the wave age (or, the nondimensional wind fetch). Anisotropy of the wave field plays a special role. By providing the necessary condition for the advective transfer of energy in the direction of the dominant wave propagation, it modifies the energy balance. In place of a purely inertial inverse cascade of the wave action with a zero spectral flux of energy (as follows from WTT for an isotropic steady state wave field [*Zakharov et al.*, 1992]), a nonconservative energy flux to the low-wavenumber range becomes possible. Ultimately, the energy is advected away from the wave generation region. One consequence is that the local dissipation by breaking waves and molecular viscosity acting at high frequencies is not the only, and probably not even a major, mechanism of energy loss. Indeed, the bulk coefficient R_q for the net energy input (wind input minus high-frequency dissipation), estimated indirectly in section 5, does not appear to be noticeably smaller than the coefficient R_q^+ for the wind input alone, estimated in Appendix B. Other, essentially nonlocal, mechanisms (wave interactions with internal waves, Langmuir circulation, mesoscale eddies, ocean currents, etc.) may be equally or even more important for the energy extraction from the wave field. Accounting for such mechanisms requires inclusion in the momentum transfer equation of terms like $\rho g(d + h)\nabla h$, where h is an averaged (over the dominant wave cycle) surface height and d may be the depth of the upper mixed layer. In the energy transfer equation, the terms like $\nabla(F\mathbf{U})$ and $\mathbf{S}(\mathbf{k}):\nabla\mathbf{U}$, where $\mathbf{S}(\mathbf{k})$ is the spectral density of the excess momentum flux tensor (including the radiation stress tensor) and $\mathbf{U}$ is the velocity field associated with ambient and wave-induced currents, are required [*Phillips*, 1977, chapter 3.6]. Depending on the nature of the "large-scale" fields h and $\mathbf{U}$, various coupled problems can be studied to identify effective mechanisms of wind-wave equilibrium. The ability of a wave field to induce larger-scale motions may have important implications for ocean-atmosphere coupling. The inclusion of an appropriate mechanism of low-frequency dissipation might also resolve the controversy related with the FDS concept.

Appendix A: Solution of (22) and (23)

Dividing (23) by (22), multiplying the result by ξ, and denoting the right-hand side of the resultant equation by $\Psi(\xi, \eta)$, we have the following transcendental equation for μ:

$$\Gamma(5/4 - \mu)/\Gamma(1 - \mu) = \Psi(\xi, \eta) \tag{A1}$$

The left-hand side can be simplified by expanding it in Taylor series about $\mu = 0$ and neglecting terms higher than μ^2. Alternatively, one can fit a quadratic polynomial to this function to find

$$\Gamma(5/4 - \mu)/\Gamma(1 - \mu) \approx 0.9058 - 0.3022\mu - 0.2295\mu^2 \tag{A2}$$

Then the solution of (22) and (23) is found in a closed form as

$$\mu \approx -0.6584 + (4.3801 - \Psi(\xi, \eta)/0.22951)^{1/2} \tag{A3}$$

Once μ has been found, $B(\xi)$ can be obtained directly from either (22) or (23).

Appendix B: Empirical Data on R_q^+

Experimentalists usually measure the spectral density q^+ of the energy flux from wind to waves and denote it by S_{in}. Unfortunately, such measurements, conducted in coastal regions, are available only for poorly developed sea states (wave age well under 1). Let us employ first an empirical form of $S_{\text{in}}(\omega)$ due to *Snyder et al.* [1981] and compare its integrated value with the net integrated energy flux Q in (34). Thus we use

$$S_{\text{in}} = H(U\omega/g - 1)\varepsilon C_q \omega(U\omega/g - 1)gF(\mathbf{k}) \tag{B1}$$

where $H(\;)$ is the unit step function and $C_q \approx 0.25$. Replacing ω with $(kg)^{1/2}$ and using (7), the integration over all wavenumbers yields

$$Q_{\text{in}} = \int S_{\text{in}}\, d\mathbf{k} = \varepsilon R_q^+ U^3 \tag{B2}$$

where the bulk coefficient of the wind energy input is

$$R_q^+ = \beta C_q[(1 - 2\mu)(3 - 4\mu)]^{-1} \tag{B3}$$

At the low degree of wave development characterizing *Snyder et al.*'s [1981] observations, the appropriate value of μ is near zero and $\beta \approx 10^{-2}$. Therefore $R_q^+ \sim 10^{-3}$ which is much greater than the value of R_q predicted in section 5. Apparently, under such conditions, the high-frequency-dissipation component of R_q is very important. The *Snyder et al.* [1981] observations were conducted in the Bay of Abaco with the local depth of 9 m and wind fetch within 10 km. Under such conditions the waves are generally steeper than those in a developed sea, which explains why these observations show large input flux.

In the observations by *Hsiao and Shemdin* [1983] in the North Sea the wave field was more mature and the corresponding empirical source function was found to be

$$S_{\text{in}} = H(U\omega/g - 1)\varepsilon C_q \omega(U\omega/g - 1)^2 gF(\mathbf{k}) \tag{B4}$$

where the empirical coefficient C_q is 0.12. The local depth, 18 m, in this experiment was still insufficient, although the fetch was greater than that in *Snyder et al.*'s [1981] experiments. *Al-Zanaidi and Hui* [1984] used (B4); however they found that the appropriate value of C_q varies between 0.04 and 0.06. It can be shown also that the empirical data summarized by *Plant* [1982] are equivalent to $C_q \approx 0.03$. *Phillips* [1985] demonstrated that C_q of this magnitude is consistent with certain other semiempirical constants characterizing wind-wave interactions, whereas larger values would lead to considerable discrepancy.

Recently, an exact regime of tetrad wave-wave interaction in the direct energy cascade, given wind input (B4), was established theoretically [*Glazman*, 1992]. The maximum value of C_q compatible with this regime follows from equation (6.12) of *Glazman* [1992]:

$$C_q = \beta^2/\varepsilon \tag{B5}$$

With $\varepsilon \approx 10^{-3}$ and $\beta \approx 5 \times 10^{-3}$, as found from Figure 9 at $\xi \approx 1$, we estimate $C_q \approx 2.5 \times 10^{-2}$. This small value lends further credibility to the suggestion that for deep-water waves considered in the present work, the correct values of C_q lie in the range 0.02–0.04, yielding $R_q^+ \approx R_q$ of section 5. In other words, the negative (high-frequency dissipation) component of the net integrated energy flux ΔQ in (33) seems to be negligible in comparison with the integrated wind input flux.

Acknowledgments. This work was performed at the Jet Propulsion Laboratory, California Institute of Technology, under contract with the National Aeronautics and Space Administration. Financial support was provided by the Office of Naval Research and NASA. The author thanks Alexander Greysukh for carrying out the data compilation and extensive calculations resulting in Figures 2–9. The help of Kenneth Steele of NDBC, who provided additional check on the condition of the buoy data used, is also gratefully acknowledged.

References

Al-Zanaidi, M. A., and W. H. Hui, Turbulent airflow over water waves—A numerical study, *J. Fluid Mech.*, *148*, 225–246, 1984.

Dobson, F., W. Perrie, and B. Toulany, On the deep-water fetch laws for wind-generated surface waves, *Atmos. Ocean*, *27*(1), 210–235, 1989.

Donelan, M. A., J. Hamilton, and W. H. Hui, Directional spectra of wind-generated waves, *Philos. Trans. R. Soc. London, Ser. A*, *315*, 509–562, 1985.

Ewing, J. A., and A. K. Laing, Directional spectra of seas near full development, *J. Phys. Oceanogr.*, *17*(10), 1696–1706, 1987.

Glazman, R. E., Statistical problems of wind-generated gravity waves arising in microwave remote sensing of surface winds, *IEEE Trans. Geosci. Remote Sens.*, *29*(1), 135–142, 1991a.

Glazman, R. E., Reply, *J. Geophys. Res.*, *96*(C3), 4979–4983, 1991b.

Glazman, R. E., Multiwave interaction theory for wind-generated surface gravity waves, *J. Fluid Mech.*, *243*, 623–635, 1992.

Glazman, R. E., and S. H. Pilorz, Effects of sea maturity on satellite altimeter measurements, *J. Geophys. Res.*, *95*(C3), 2857–2870, 1990.

Glazman, R. E., and M. A. Srokosz, Equilibrium wave spectrum and sea state bias in satellite altimetry, *J. Phys. Oceanogr.*, *21*(11), 1609–1621, 1991.

Glazman, R. E., and P. Weichman, Statistical geometry of a small surface patch in a developed sea, *J. Geophys. Res.*, *94*(C4), 4998–5010, 1989.

Glazman, R. E., G. G. Pihos, and J. Ip, Scatterometer wind speed bias induced by the large-scale component of the wave field, *J. Geophys. Res.*, *93*(C2), 1317–1328, 1988.

Grose, P. L., K. L. Warsh, and M. Garstang, Dispersion relations and wave shapes, *J. Geophys. Res.*, *77*(21), 3902–3906, 1972.

Hasselmann, K., On the non-linear energy transfer in a gravity-wave spectrum, *J. Fluid Mech.*, *12*, 481–500, 1962.

Hasselmann, K., et al., Measurements of wind wave growth and swell decay during the Joint North Sea Wave Project (JONSWAP), *Deutsch. Hydrograph. Z.*, *8*(12), suppl. A, 95 pp., 1973.

Hsiao, S. V., and O. H. Shemdin, Measurements of wind velocity and pressure with a wave follower during MARSEN, *J. Geophys. Res.*, *88*(C14), 9841–9849, 1983.

Kahma, K. K., A study of the growth of the wave spectrum with fetch, *J. Phys. Oceanogr.*, *11*(11), 1503–1515, 1981.

Kitaigorodskii, S. A., Applications of the theory of similarity to the analysis of wind-generated wave motion as a stochastic process, *Bull. Acad. Sci. USSR, Geophys. Ser.*, Engl. Transl., no. 1, 105–117, 1962.

Kitaigorodskii, S. A., *Fizika vzaimodeistviya atmosfery i okeana* (in Russian), Gidrometeoizdat, St. Petersburg, Russia, 1970. (English

translation, *Physics of Air-Sea Interaction*, Israel Program for Scientific Translation, Jerusalem, 1973.)
Kitaigorodskii, S. A., On the theory of the equilibrium range in the spectrum of wind-generated gravity waves, *J. Phys. Oceanogr.*, *13*(5), 816–827, 1983.
Liu, P. C., and D. B. Ross, Airborne measurements of wave growth for stable and unstable atmospheres in Lake Michigan, *J. Phys. Oceanogr.*, *10*(11), 1842–1853, 1980.
Mitsuyasu, H., R. Nakayama, and T. Komori, Observations of the wind and waves in Nakata Bay, *Rep. Res. Inst. Appl. Mech. Kyushu Univ.*, *19*, 37–74, 1971.
Murphy, J. E., NDBO large discus and Nomad buoy calibrations with WRANSAC, *Oceans'79*, 221–225, 1979.
Phillips, O. M., *The Dynamics Of The Upper Ocean*, 2nd ed., 336 pp., Cambridge University Press, New York, 1977.
Phillips, O. M., Spectral and statistical properties of the equilibrium range in wind-generated gravity waves, *J. Fluid Mech.*, *156*, 505–531, 1985.
Pierson, W. J., Comment on "Effects of sea maturity on satellite altimeter measurements" by R. E. Glazman and S. H. Pilorz, *J. Geophys. Res.*, *96*(C3), 4973–4977, 1991.
Pierson, W. J., and L. Moskowitz, A proposed spectral model for fully developed wind seas based on the similarity theory of S. A. Kitaigorodskii, *J. Geophys. Res.*, *69*(24), 5181–5190, 1964.
Plant, W. J., A relationship between wind stress and wave slope, *J. Geophys. Res.*, *87*(C3), 1961–1967, 1982.
Ross, D. B., On the use of aircraft in the observation of one- and two-dimensional ocean wave spectra, in *Ocean Wave Climate*, edited by M. D. Earle and A. Malahoff, pp. 253–267, Plenum, New York, 1978.
Snyder, R. L., F. W. Obson, J. A. Elliot, and R. B. Long, Array measurements of atmospheric pressure fluctuations above surface gravity waves, *J. Fluid Mech.*, *102*, 1–59, 1981.
Toba, Y., Local balance in the air-sea boundary processes, III, On the spectrum of wind waves, *J. Oceanogr. Soc. Jpn.*, *29*, 209–220, 1973.
Walsh, E. J., D. W. Hanckock III, D. E. Hines, R. N. Swift, and J. F. Scott, An observation of the directional wave spectrum evolution from shoreline to fully developed, *J. Phys. Oceanogr.*, *19*(5), 670–690, 1989.
Zakharov, V. E., and N. N. Filonenko, The energy spectrum for stochastic oscillation of a fluid's surface (in Russian), *Dokl. Akad. Nauk SSSR*, *170*(6), 1292–1295, 1966.
Zakharov, V. E., and M. M. Zaslavskii, The kinetic equation and Kolmogorov spectra in the weak turbulence theory of wind waves, *Izv. Acad. Sci. USSR Atmos. Oceanic Phys.*, English Transl., *18*(9), 747–753, 1982.
Zakharov, V. E., and M. M. Zaslavskii, Dependence of wave parameters on the wind velocity, duration and its action and fetch in the weak-turbulence theory of wind waves, *Izv. Acad. Sci. USSR Atmos. Oceanic Phys.*, English Transl., *19*(4), 300–306, 1983.
Zakharov, V. E., V. S. L'vov, and G. Falkovich, *Kolmogorov Spectra of Turbulence: Wave Turbulence*, 280 pp., Springer-Verlag, New York, 1992.

R. E. Glazman, Jet Propulsion Laboratory, California Institute of Technology, 4800 Oak Grove Drive, Pasadena, CA 91109-8099. (e-mail: Internet.reg@foggy.jpl.nasa.gov)

(Received February 2, 1993; revised October 18, 1993; accepted November 4, 1993.)